J. Mol. Model. **1996**, *2*, 278 – 285

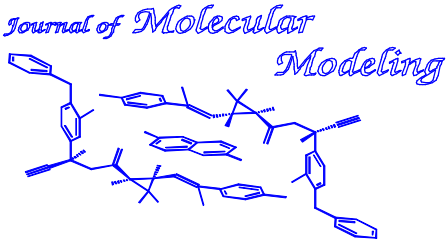

NpH-MD-Simulations of the Elastic Moduli of Cellulose II at Room Temperatue

Johannes Ganster*

Fraunhofer Institute of Applied Polymer Research, Kantstrasse 55, D-14513 Teltow-Seehof, Germany (ganster@iap.fhg.de)

John Blackwell

Department of Macromolecular Science, Case Western Reserve University, Cleveland, Ohio 44106-7202, USA.

Received: 15 May 1996 / Accepted: 6 August 1996 / Published: 27 September 1996

Abstract

We have used molecular dynamics modeling to investigate the stucture and mechanical properties of regenerated cellulose fibres. This work is motivated by continued interest in replacing the environmentally hazardous viscose process by alternative spinning methods. An important input parameter for any realistic model of the elastic properties is the stiffness tensor of the crystalline constituent, cellulose II. Conventional molecular mechanics techniques can be used to estimate the elastic reaction of a material with respect to small external stresses or strains, i.e. the compliance and stiffness tensors, and the elastic moduli derived therefrom, at zero temperature. In order to access non-zero temperatures, it is necessary to use either the quasi-harmonic approximation for the vibrational free energy or molecular dynamics (MD) simulations. In the present work, Parrinello-Rahman constant-stress MD was performed to generate trajectories in constant particle number (N), constant external stress tensor (p or **t**) and constant enthalpy H (NpH or H**t**N) ensemble. This was found to be less time consuming than working with isothermal conditions, as done by other authors. The fluctuations in kinetic energy and MD cell vectors were then used to calculate adiabatic elastic constants, thermal expansion coefficients and heat capacity. The isothermal elastic constants were found by applying a standard thermodynamic relation. The Young's modulus along the chain direction, E_l, was determined to be 155 GPa, whereas the values in the perpendicular directions vary between 51 and 24 GPa. These results are of the same order of magnitude as those obtained by Tashiro and Kobayashi [1] with the static (T = 0K) method, but our value of E_l is 5% lower and, unexpectedly, the lateral values are up to six times higher. A strong anisotropy is found for shear along the chains in planes containing the chain axis, the shear modulus ranging from 5 to 20 GPa. Convergence was achieved in the simulations, to the extend that the elastic constants become stationary, but significant internal stresses remain, pointing to shortcomings in the software used. Further work is necessary to resolve these problems, although the major conclusions should be unaffected.

Keywords: material modeling, molecular mechanics, MD

* *To whom correspondence should be addressed*

Introduction

The cellulose II polymorphic structure [2, 3] is characteristic of regenerated or Mercerized cellulose fibers. The mechanical properties of these materials depend on the structure of the individual molecules and their mutual interactions, to the degree to which an optimum structure has been attained [4]. One of the most simple sets of parameters describing the mechanical behavior of an array of polymer chains consists of the components of the three-dimensional small strain elastic constant or stiffness matrix **C,** and their reciprocals, i.e. the compliances, $\mathbf{S} = \mathbf{C}^{-1}$. Cellulose II has an approximately monoclinic $P2_1$ space group, which has 13 independent stiffness components [5]. A full experimental determination of these parameters is out of the question, but the Young's modulus of fibres can be determined by following the stress induced shifts of the X-ray diffraction peaks due to lattice deformation, provided that the relation between external load and local crystalline stress is known (or can reasonably be assumed). Estimates of E_ℓ for semicrystalline, regenerated cellulose fibers are reported in the range of 70 - 112 GPa [6-9].

Theoretical calculations employing appropriate force fields allow the determination of the whole stiffness tensor [10]. For cellulose, such calculations have been performed by Tashiro and Kobayashi [1], leading to a value for E_ℓ for cellulose II of 162 GPa [10]. A considerably lower value of 86 GPa was obtained by Kroon-Batenburg *et al.* [11], who considered only a single chain and used a markedly different force field. The main shortcoming of such calculations is their static character, i.e. the mechanical parameters are calculated for the minimum energy structure, which is effectively for 0 K.

Non-static methods for the calculation of stiffness tensors at non-zero temperatures have only recently been applied to polymer crystals. Lacks and Rutledge [12] have used the quasi-harmonic approximation for the vibrational free energy (in both the classical and quantum mechanical formulations) to allow for the thermal vibrations of the atoms, and have calculated the stiffness tensor for polyethylene at several temperatures in the range from 0 to 400 K. Gusev *et al.* [13-15] have employed Parrinello-Rahman constant-stress molecular dynamics (MD) [16] with a Nosé-Hoover thermostat [17, 18] to calculate isothermal stiffness tensors for polyethylene from the corresponding fluctuation formula [19].

In the present work, Parrinello-Rahman MD simulations have been performed for cellulose II in order to calculate the adiabatic stiffness, thermal expansion and heat capacity using the fluctuation formulae due to Ray [20]. In contrast to the work of Gusev *et al.* [13-15], we have employed less time consuming simulations utilizing a constant enthalpy H, tension **t** and particle number N (H**t**N) ensemble. The isothermal stiffness tensor was calculated from standard thermodynamic relations [21].

Method

According to Andersen [22], Parrinello and Rahman [16], and Ray [23, 24], MD in a scaled and augmented Hamiltonian system can be used to simulate constant stress conditions. This leads to a time-dependent MD cell with fluctuating cell vectors **a**, **b**, **c,** which are summarized in the cell matrix **h**:

$$\mathbf{h} = \begin{pmatrix} a_1 & b_1 & c_1 \\ a_2 & b_2 & c_2 \\ a_3 & b_3 & c_3 \end{pmatrix}$$

and is used to calculate the instantaneous strain tensor γ:

$$\varepsilon = \frac{1}{2}(\mathbf{h}_0'^{-1}\mathbf{h}'\mathbf{h}\mathbf{h}_0^{-1} - 1) \qquad (1)$$

Here, h_0 is the average h matrix in a zero stress situation, and the prime indicates matrix transposition. The instantaneous and average volumes, V and V_0, are given by the determinants $V = \det(h)$ and $V_0 = \det(h_0)$, respectively.

The microscopic stress tensor, σ, is calculated from

$$\sigma = \frac{1}{V}\left[\sum_a \frac{\mathbf{p}_a' \circ \mathbf{p}_a}{m_a} + \sum_{a<b} \mathbf{f}_{ab}' \circ (\mathbf{r}_a - \mathbf{r}_b)\right] \qquad (2)$$

where

$$\mathbf{f}_{ab} = -\frac{\partial U(\{\mathbf{r}_c - \mathbf{r}_d\})}{\partial(\mathbf{r}_a - \mathbf{r}_b)}$$

is the derivative of the potential energy function U of the system, which depends on the set $\{\mathbf{r}_c - \mathbf{r}_d\}$ of the interatomic distance vectors between atoms *c* and *d* at positions $\mathbf{r}_c$ and $\mathbf{r}_d$ in the unscaled system and ∘ means the dyadic product for vectors. The linear momentum $\mathbf{p}_a$ of atom *a* with mass m_a is also taken in the unscaled system, and is different from the time derivative of $\mathbf{r}_a$ [23]. For molecular systems the angle bending and torsional forces are not central, with a result that $\mathbf{f}_{ab}$ is not parallel to $\mathbf{r}_a - \mathbf{r}_b$, giving a non-symmetric instantaneous stress tensor [25, 26].

We define $\delta(ab)$ as the fluctuation of two quantities *a* and *b* according to

$$\delta(ab) = \langle ab \rangle - \langle a \rangle \langle b \rangle$$

where <...> designates the H**t**N ensemble average, which is equal to the trajectory average after equilibration. The

adiabatic elastic constant (stiffness) tensor **C** is given by [16]

$$\delta(\varepsilon_{ij}\varepsilon_{kl}) = \frac{kT}{V} C^{-1}_{ijkl}, \tag{3}$$

where T=2<K>/3Nk is the instantaneous temperature and $K = \Sigma p_a^2/2m_a$ is the kinetic energy, k is Boltzmann's constant, and N is the number of atoms. The heat capacity C_p and the thermal expansion tensor, α^p (both for constant stress), can be determined [20] from

$$\delta(K^2) = \frac{3}{2} N(kT)^2 \left[1 - \frac{3Nk}{2C_p}\right], \tag{4}$$

$$\delta(\varepsilon_{ij}K) = -\frac{3}{2} N(kT)^2 \frac{1}{C_p} \alpha^p_{ij}, \tag{5}$$

allowing for calculation of the isothermal elastic stiffness, ^TC[21]

$$^T C^{-1}_{ijkl} = C^{-1}_{ijkl} + V_0 \frac{T\alpha^p_{ij}\alpha^p_{kl}}{C_p}. \tag{6}$$

To control the convergence to equilibrium, Gusev *et al.* [13] compared averaged stress-strain products (invariants) with their equilibrium values (0, 0.5 and 1) according to

$$\frac{V}{kT}\langle \sigma_{ij}\varepsilon_{kl}\rangle = \frac{\delta_{ik}\delta_{jl} + \delta_{il}\delta_{jk}}{2}, \tag{7}$$

where δ_{ij} is the Kronecker symbol: δ_{ij} = 1 for $i = j$ and 0 otherwise.

Experimental

Molecular models for cellulose II were based on the X-ray work by Kolpak and Blackwell [2], which is similar to the structure also proposed by Stipanovich and Sarko [3]. The structure is described by a monoclinic unit cell (space group $P2_1$) with dimensions a = 8.01 Å, b = 9.04 Å, c (fiber axis) = 10.36 Å, and γ = 117.1° [2], containing disaccharide units of two chains of opposite sense that pass through the origin and center of the *ab* projection. As described in refs. 2 and 3, the two chains have identical backbone conformations, but differ in the conformations of the CH_2OH side chains, which are *gauche-trans (gt)* on one chain and *trans-gauche (tg)* on the other. Recent work by Gessler et al. [27] has determined the structure of cellotetraose by single crystal methods, which is thought relevant to cellulose II because of the close similarity of the polymer and

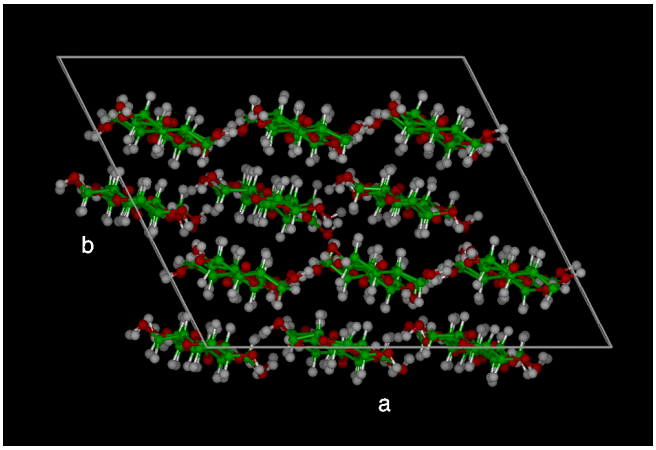

Figure 1. *Snapshot of the simulated cellulose II MD cell containing 12 cellulose chains of four anhydroglucose units, viewed along the* c *direction.*

tetramer unit cells. In the cellotetraose unit cell, the two molecules have the same CH_2OH conformations *(gt)*, but have slightly different backbone conformations. We have elected to retain the published cellulose II structure as the starting model. However, there is more than sufficient freedom for rearrangement to the all-*gt* model during the dynamic modeling, and it will be seen that such a change does not in fact occur.

Construction of the molecular models, energy minimization and MD was accomplished using the Biosym molecular modeling software [28] on a Silicon Graphics Power Series 4D 220 GTXB computer. A unit cell was constructed according to the structural features described above, us-

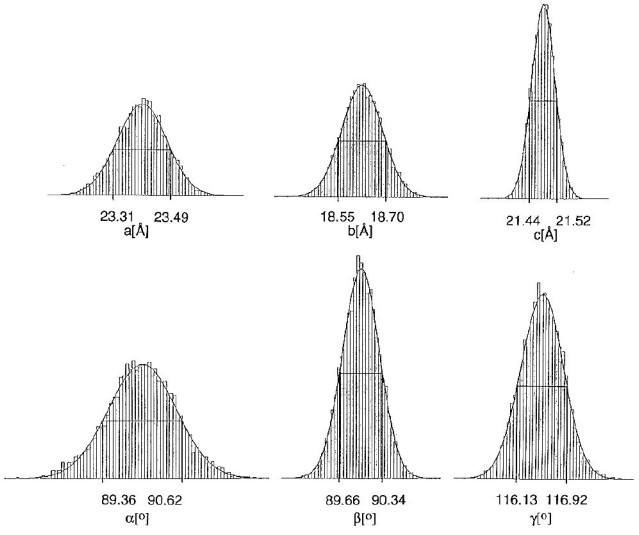

Figure 2. *Frequency distribution of MD cell lengths* a, b,c *and angles* α, β, γ *in a 100 ps HtN run. The solid lines are best fit Gaussian distributions for these data.*

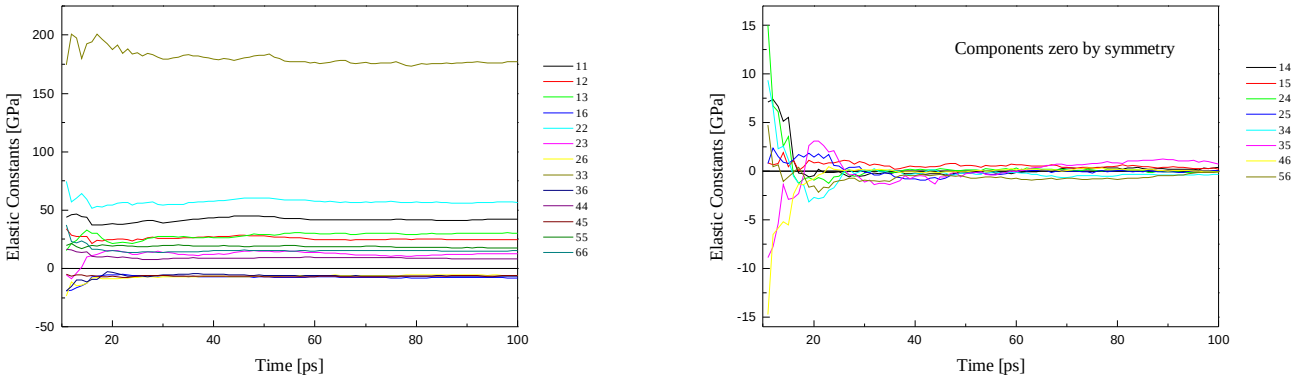

Figure 3. *Running averages of the adiabatic elastic constants (components of* ***C****) obtained by H**t**N-MD after 440 ps of relaxation. left: non-zero components; right: components predicted to be zero by symmetry.*

ing the default molecular geometry contained in the software package [28] except that the torsion angles at the glycosidic linkages, the CH_2OH conformations, and the mutual stagger of the center and corner chains along the *z* axis were taken from reference [2]. The force field was chosen by comparing energy minimizations with periodic boundary conditions (pbc) for the unit cell with variable cell dimensions using the CVFF [29, 30], PCFF [31] and AMBER [32-34] force fields from the DISCOVER program [28]. All three force fields produced structures similar to that in reference [2] with deviations in *a*, *b*, *c* and γ of less than 5 % (α and β were very close to 90°). The calculated density was always somewhat lower than the experimental value of 1.61 g/cm^3, but this difference did not exceed 5 %. Even a perfect match in the static structure would not assure the quality of the force field in dynamic simulations. Since there was little difference between the results using different force fields, we used the original CVFF force field.

The MD cell consisted of three unit cells in the *a* direction and two each in the *b* and *c* directions. (The use of larger cells resulted in prohibitive long calculation times.) The simulations were performed with application of periodic boundary conditions (pbc) in the H**t**N mode, these being three times faster than isothermal ensemble calculations. A time step of 1 fs was used together with a charge group-based cutoff of 9.5 Å (full interaction up to 8.5 Å) both for van der Waals and Coulombic forces, a dielectric constant of 1, default bond increments of the force field for assigning net atomic charges, a cell mass parameter of 20 atomic units, and the velocity Verlet integrator [28]. Simulations were carried through up to 540 ps. Cross terms were not included in the force field and a simple quadratic potential was used instead of a Morse term for the bond length oscillations. A starting temperature of 602 K was found appropriate to reach the target temperature of 298 K. However, a slight heating up to 303.5 K after 500 ps was observed. After some 10 ps, the average shape of the MD cell reached the final form described by the average unit cell dimensions given in *Table 1*. The relatively large *c* value of 10.74 Å as compared to the experimental value of 10.36 Å [2] is viewed as a defect of the force field, but is not expected to have more than a minor influence on the results of the simulations.

The quantities of interest: cell parameters, kinetic energy and instantaneous microscopic stress tensor determined by the DISCOVER program [28] were saved every 10 fs. Our coordinate system has the same orientation as that of Tashiro and Kobayashi [1], i.e. the *c* axis is parallel to *z* and the *b* axis lies in the *z y* plane. The contracted notation [5] for tensor indices (11->1, 22->2, 33->3, 23->4, 13->5, 12->6) is used for fourth rank tensors. The cell matrix **h** was constructed from the cell parameters, and $\mathbf{h}_0$ was obtained by averaging **h** over the whole run. **ε** was calculated according to eq. (1) for every tenth point on the trajectory.

Table 1. *Density Δ, unit cell lengths a, b, c and angles α, β, γas determined by X-ray structure analysis [2] and the present MD calculations as well as relative deviations)*

	ρ [g/cm^3]	**a [Å]**	**b [Å]**	**c [Å]**	**α [°]**	**β [°]**	**γ [°]**
X-ray [1]	1.61	8.01	9.04	10.36	90	90	117.1
MD	1.54	7.80	9.31	10.74	90	90	116.6
Δ [%]	-5	-3	3	4	-	-	-1

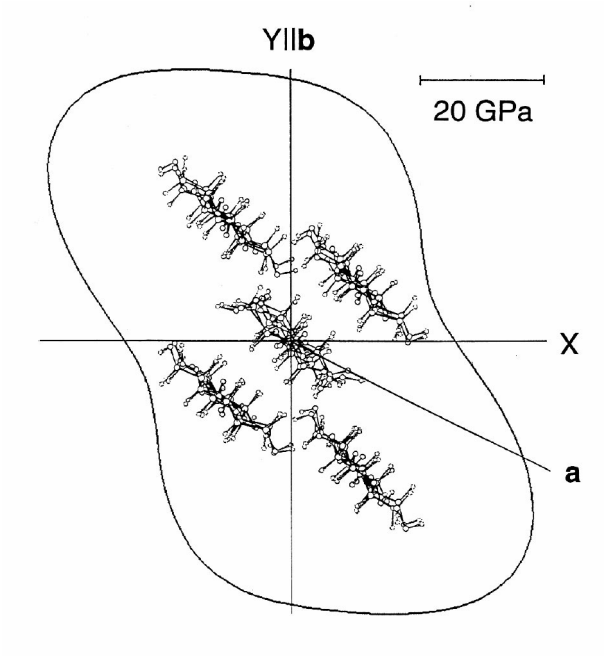

Figure 4. *Young's modulus perpendicular to the chain direction as a function of orientation. The distance from the origin to the bold line is proportional to the modulus.*

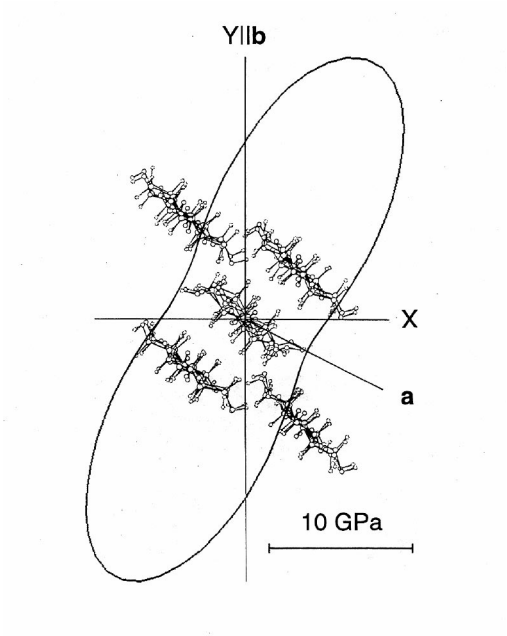

Figure 5. *Shear modulus for the planes containing the* c *axis as a function of orientation. The distance from the origin to the bold line in a given direction is proportional to the modulus for shear along* c *in the plane containing* c *and that direction.*

Results and Discussion

A snapshot of the MD cell at 300 K after 540 ps of simulation time viewed along the chain direction *c* is shown in Figure 1. A short animation of the trajectory of the system showed that the hydrogen bond system as described in [2] and [3] is essentially maintained. As mentioned above, the structure does not rearrange to the all-*gt* bonding scheme found in the crystal structure of cellotetraose by single crystal determination [27].

Table 2. *Young's moduli* E_i, *Poisson ratios* ν_{ij} *and shear moduli* G_i *as calculated from the stiffness constant tensor* **C**

E_1[GPa]	E_2[GPa]	E_ℓ[GPa]	ν_{12}	ν_{13}	ν_{21}
26.4	42.2	154.6	0.37	0.13	0.59

ν_{23}	ν_{31}	ν_{32}	G_1[GPa]	G_2[GPa]	G_3[GPa]
-0.03	0.78	-0.12	13.5	12.6	5.9

Figure 2 shows the frequency distribution of the MD cell lengths and angles over a 100 ps run (i.e. 10000 data points). It can be seen that there are good fits to the best (least squares) Gaussian distributions, indicating an appropriate choice of the cell mass parameter. As is to be expected, the covalent bonds of the polymer chains restrict the cell motion in the *c* direction; there is more freedom in the non bonded directions, and *a* shows a slightly broader distribution than *b*. The „weakest" unit cell angle is α, indicating a relatively easy gliding of the *020* planes past each other, which is consistent with the anisotropy of the shear modulus (see below).

Figure 3 shows running averages of the 13 non-zero and the 8 vanishing adiabatic elastic constants calculated according to eq. (3) for a 100 ps run starting after 440 ps of relaxation. The final values averaged over 100 ps after 540 ps are

$$C = \begin{pmatrix} \mathbf{42.2} & \mathbf{24.5} & \mathbf{30.0} & 0.4 & 0.2 & \mathbf{-8.1} \\ \mathbf{24.5} & \mathbf{56.7} & \mathbf{12.5} & -0.1 & 0.0 & \mathbf{-5.9} \\ \mathbf{30.3} & \mathbf{12.5} & \mathbf{177.2} & -0.3 & 0.7 & \mathbf{-6.8} \\ 0.4 & -0.1 & -0.3 & \mathbf{8.1} & \mathbf{-6.2} & -0.1 \\ 0.2 & 0.0 & 0.7 & \mathbf{-6.2} & \mathbf{17.3} & -0.1 \\ \mathbf{-8.1} & \mathbf{-5.9} & \mathbf{-6.8} & -0.1 & -0.1 & \mathbf{15.1} \end{pmatrix} GPa \cdot$$

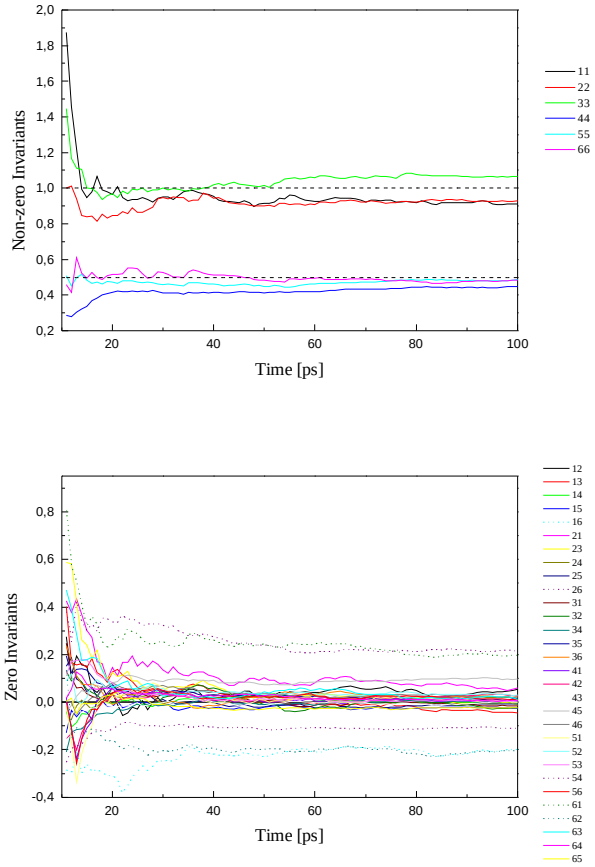

Figure 6. *Running averages of diagonal (above) and non-diagonal (below) invariants $V<\sigma_{ij}\varepsilon_{kl}>/(kT)$. Relatively large deviations from zero are seen in for the 16, 61, 26, 62, 45 and 54 components.*

The components predicted to be zero on the basis of symmetry are shown in non-bold face. The value of E_ℓ = 155 GPa calculated from this stiffness matrix is slightly lower than the value of 162 GPa determined by Tashiro and Kobayashi for 0 K [1]. None of our figures for the non-vanishing components are as close to zero as are those for C_{13}, C_{16}, C_{23} and C_{36} reported by Tashiro and Kobayashi [1]. Except for the stiffness in chain direction, (C_{33}), the remaining components in the present work are two to six times higher. This may be due to differences in the force field or an effect of disregarding the lack of symmetry in the microscopic stress tensor in the Biosym software [28] (see below). The stiffness components for cellulose II other than C_{33} are also comparatively high compared to those reported (5 - 9 GPa) in simulations of polyethylene and isotactic polypropylene [13, 14], most probably due to the rich hydrogen bond system maintained in the present room temperature simulations. The Young's moduli, Poisson ratios and shear moduli as calculated from the stiffness tensor **C** are given in Table 2.

The directional dependence of the Young's modulus perpendicular to the chain direction E_φ([1], [5]) as calculated from **C** is visualized in Figure 4, where the distance from the origin to the bold line is proportional to the modulus in that direction. The „stiffest" direction is close to $[1\bar{1}0]$, where deformation requires stretching or compressing the hydrogen bonds, for which the modulus is 51.4 GPa. The „most compliant" direction is close to *[110]*, where a change in the O-H···O bond angle would be sufficient to allow deformation, and has a modulus of 23.9 GPa.

Figure 5 shows an analogous plot of the shear modulus G(φ) [5] for planes containing the chain direction with respect to forces along this direction. n is the inclination angle of the shear plane with the *x* axis, i.e. G_{23} is found along the *x* axis and G_{13} along the *y* axis. The anisotropy is seen to be even more pronounced than that for E_φ. G = 20.0 GPa close to the $\bar{1}10$ plane, which is stabilized in many ways by valence forces. This is about four times greater than the value for shear close to the weaker bound *110* sheets. Our predictions correlate with the comparatively broad frequency distribution for α in Figure 2.

The running averages of the invariants according to eq. (7) are shown for the last 90 ps of the simulation in Figure 6. The values at the end of the run are

$$\frac{2V}{kT}\langle\sigma\varepsilon\rangle = \begin{pmatrix} \mathbf{0.91} & 0.05 & -0.05 & -0.01 & -0.02 & -0.20 \\ 0.06 & \mathbf{0.93} & -0.01 & -0.02 & -0.01 & 0.22 \\ -0.01 & -0.02 & \mathbf{1.07} & 0.00 & 0.01 & 0.02 \\ 0.00 & 0.03 & 0.00 & \mathbf{0.45} & 0.1 & 0.02 \\ 0.00 & 0.03 & 0.01 & -0.11 & \mathbf{0.49} & 0.01 \\ 0.20 & -0.20 & 0.01 & 0.01 & -0.02 & \mathbf{0.48} \end{pmatrix}.$$

Ideally, the off-diagonal terms should be zero. However, the 16, 61, 26, 62, 45 and 54 components deviate considerably from their equilibrium values of zero and show no tendency to converge further. (The same effect was noticed in earlier runs, from 240 to 340 and from 340 to 440 ps). In addition, the microscopic stress tensor output by the Biosym DISCOVER program [28] (which gives only six components, thus assuming the tensor to be symmetric) does not converge to zero after 540 ps for our **t** = 0 simulation, as shown in Figure 7. Similar problems have been encountered in a constant stress isothermal simulation of isotactic polypropylene crystals [35]. Furthermore, the average of $\boldsymbol{\sigma}\mathbf{V}\mathbf{h}'^{-1}$ gave non-zero values. This is not the correct behaviour, as one can see by averaging the differential equation for **h** [36]. A variation of the cell mass parameter did not lead to significantly different results, suggesting that the above effect is not due to incomplete convergence. The asymmetrical rotational components of the cell dynamics could not be studied because the cell tensor **h** is not evaluated as such, but has to be recalculated from the MD cell dimensions. However, these problems relate

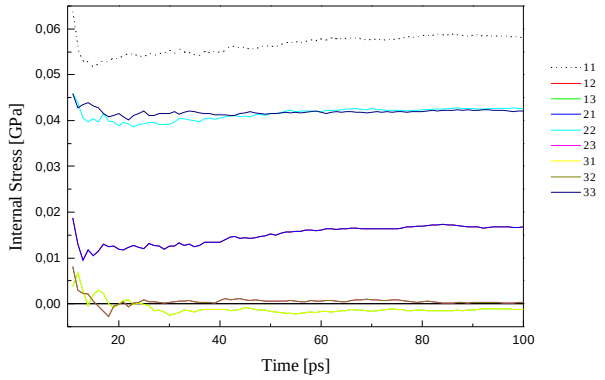

Figure 7: *Running averages of microscopic internal stresses for the simulation shown in Figure 3.*

to the rotational motion. Only fluctuations are necessary to calculate the elastic constants, and these should not be affected more than the invariants shown in Figure 6.

The final values for the specific heat and the thermal expansion are, respectively, c_p= 3.3 J/(gK) and

$$\alpha^p = \begin{pmatrix} 4.3 & -1.2 & 0.1 \\ -1.2 & 0.7 & 1.0 \\ 0.1 & 1.0 & 0.1 \end{pmatrix} 10^{-5} / K$$

giving a bulk expansion of α_{ii} = 5.1 10^{-5}/K and an averaged linear isotropic expansion of α = 1.7 10^{-5}/K. The specific heat is somewhat higher and the expansion coefficient lower than the values reported [37] for cellulose acetate (c_p = 1.3 J/(gK), α= 14 10^{-5}/K) and cellulose acetate butyrate (c_p = 2.1 J/(gK), α = 12.5 10^{-5}/K), but the latter are amorphous materials. A low thermal expansion must be expected for the mainly quadratic force field, especially for the bonded interactions: complete absence of anharmonic terms would result in no thermal expansion at all. Using the thermodynamic relation [20, 21]

$$\frac{c_p}{c_v} = 1 + \frac{V_0 T \alpha_{ij}^p \alpha_{kl}^p C_{ijkl}}{C_p} \qquad (8)$$

we obtain a value of 3.25 J/(gK) for c_v from the present fluctuation calculations, which is very close to that of 3.23 J/(gK) derived using the Dulong and Petit law [38]. This suggests that the errors due to low α^p and high stiffness tend to cancel out in eq. (8).

Calculating the isothermal stiffness using eq. (6) gave ^{T}**C** values lower than the corresponding **C** components, but within the scatter of components which should be zero by symmetry, i.e. there is no significant difference between **C** and ^{T}**C**. A comparison with the constant temperature simulations (T**t**N ensemble) could reveal deficiencies in the force field and/or the sampling method.

Conclusions

Room temperature adiabatic elastic constants, thermal expansion coefficients and heat capacity of cellulose II have been calculated using constant stress molecular dynamics. During the simulation, the system remained close to the starting configuration, maintaining a dense hydrogen bond network very similar to that found by X-ray crystal structure analysis. Compared to other polymers, the lateral stiffness of cellulose II is high, which is most probably due to the intra- and inter- molecular hydrogen bond system. The isothermal elastic constants do not differ from the adiabatic values within the limitations of the calculation. Thermal expansion coefficients are somewhat low, whereas the specific heat is found to be almost exactly that of Dulong and Petit's rule.

Although convergence was achieved in the sense that the stiffness tensor remains constant for prolonged simulation times, terms in the averaged microscopic stress tensor differ considerably from their expected zero values and showed no tendency to converge further. It seems likely that this was caused by the use of a symmetric instantaneous stress tensor in in the commercial software used.

Acknowledgement: The support of the German Academic Exchange Service through a fellowship to J. Ganster is gratefully acknowledged.

References

1. Tashiro, K. and Kobayashi, M. *Polymer* **1991**, *32*, 1516-1526.
2. Kolpak, F.J. and Blackwell, J. *Macromolecules* **1976**, *9*, 273-278.
3. Stipanovic, A.J. and Sarko, A. *Macromolecules* **1976**, *9*, 851-857.
4. Ganster, J.; Fink, H.-P.; Fraatz, J. and Nywlt, M. *Acta Polym.* **1994**, *45*, 312-318.
5. Hearmon, R.F.S. *An Introduction to Applied Anisotropic Elasticity*, Oxford Univ. Press, 1961.
6. Mann, J. and Roldan-Gonzalez, L. *Polymer* **1962**, *3*, 549-553.
7. Sakurada, I., Ito; T. and Nakamae, K. *Macromol. Chem.* **1964**, *75*, 1-10.
8. Matsuo, M.; Sawatari, Ch.; Iwai, Y. and Ozaki, F. *Macromolecules* **1990**, *23*, 3266-3275.
9. Nishino, T.; Takano, K. and Nakamae, K. *J. Polym. Sci. B, Polym. Phys.* **1995**, *33*, 1647-1651.

10. Tashiro, K.; Kobayashi, M. and Tadokoro, H. *Macromolecules* **1978**, *11*, 908-913.
11. Kroon-Batanburg, L.M.J.; Kroon, J. and Northolt, M.G. *Polymer* **1986**, *27*, 290-292.
12. Lacks, D.J. and Rutledge, G.C. *J. Phys. Chem.* **1994**, *98*, 1222-1231.
13. Gusev, A.A.; Zehnder, M.M. and Suter, U.W. *J. Chem. Phys.* submitted for publication.
14. Gusev, A.A.; Zehnder, M.M. and Suter, U.W. presented at the ACS short Course Molecular *Modeling of Polymers*, 1.-2.7.1994, Akron, OH.
15. Gusev, A.A.; Zehnder, M.M. and Suter, U.W. *Macromolecules* **1994**, *27*, 615-616.
16. Parrinello, M. and Rahman, A. *J. Appl. Phys.* **1981**, *52*, 7182-7190.
17. Nosé, S. *Mol. Phys.* **1984**, *52*, 255-268; *J. Chem. Phys.* **1984**, *81*, 511-519.
18. Hoover, W.G. *Phys. Rev.* **1985**, *A31*, 1695-1697.
19. Parrinello, M. and Rahman, A. *J. Chem. Phys.* **1982**, *76*, 2662-2666.
20. Ray, J.R. *J. Appl. Phys.* **1982**, *53*, 6441-6443
21. Thurston, R.N. in *Physical Acoustics*, Vol. I, Part A, W.P. Mason (Ed.) Academic, New York 1964, p. 39.
22. Andersen, H.C. *J. Chem. Phys.* **1980**, *72*, 2384-2393.
23. Ray, J.R. and Rahman, A. *J. Chem. Phys.* **1984**, *80*, 4423-4428
24. Ray, J.R. *Comp. Phys. Reps.* **1988**, *8*, 109-152.
25. Nosé, S. and Klein, M.L. *Mol. Phys.* **1983**, *5*, 1055-1076.
26. Theodorou, D.N.; Boone, T.D.; Dodd, L.R. and Mansfield, K.F. *Macromol. Chem., Theory Simul.* **1993**, *2*, 191-238.
27. Gessler, K.; Krauss, N.; Steiner, Th.; Betzel, Ch.; Sandmann, C. and Saenger, W. *Science* **1994**, *266*, 1027-1029.
28. *Insight II 2.3.0*, *Polymer 6.0*, *Discover 94.0* available from Biosym Technologies, Inc. San Diego, CA, 1994.
29. Lifson, S.; Hagler, A.T. and Dauber, P. *J. Am. Chem. Soc.* **1979**, *101*, 5111-5121.
30. Hagler, A.T.; Lifson, S. and Dauber, P. *J. Am. Chem. Soc.* **1979**, *101*, 5122-5130 and 5131-5141.
31. Maple, J.R.; Hwang, H.-J.; Stockfisch, T.P.; Dinur, U.; Waldman, M.; Ewis, C.S. and Hagler, A.T. *J. Comp. Chem.* **1994**, *15*, 162-166.
32. Weiner, S.J.; Kollman, P.A.; Case, D.; Singh, U.C.; Ghio, C.; Alagona, G.; Profeta, S. Jr. and Weiner, P. *J. Am. Chem. Soc.* **1984**, *106*, 765-784.
33. Weiner, S.J.; Kollman, P.A.; Nguyen, D.T. and Case, D.A. *J. Comp. Chem.* **1986**, *7*, 230-252.
34. Homans, S.W. *Biochemistry* **1990**, *29*, 9110-9118.
35. Suter, U.W. personal communication.
36. Ray, J. *J. Chem. Phys.* **1983**, *79*, 5128-5130.
37. Encyclopedia of Poymer Science and Engineering, Vol. 16. John Wiley & Sons, New York, 1989, p. 737.
38. Becker, R. *Theory of Heat*, Springer-Verlag, New York, 1967, p. 234.